UNIVERSITÉ DE NANTES

Master 1 - Statistical Engineering

Supervised Study Project in Mathematics

Gaussian space field simulations

Author :
Aymeric
Lechevranton
Pierre-Emmanuel
Séchet
Makhète Cisse

Adviser :
Nicolas Bez

May 24, 2019

Abstract

This paper addresses the problem of simulating a Gaussian random field. Several approaches of simulation are depicted and implemented on the software environment R. Our goal is to analyze the results of the simulation especially with the variogram.

Keywords: Gaussian random field, Covariance, Variogram, Cholesky Decomposition, Spectral method, Turning bands.

We would like to thank sincerely our supervisor Nicolas Bez for his patience and the time he spent with us to advise and help us.

Contents

1 Introduction

Several kinds of random fields exist : the Markov random field, the Gibbs random field or the Gaussian random field. This report consists in simulating Gaussian random fields in different ways. In order to achieve this, the first part introduces the essential notions of the random fields and their properties. We will address also the way to analyze a random field. The second part is on the main methods of simulations. We will create Gaussian random fields with the Cholesky method and the Turning bands method. Then we will value the convergence of the experimental variograms to the theoretical variogram. We will also analyze the variability of the experimental variograms around the theoretical one to appreciate the characteristics of the Gaussian random field.

If you want to explore the concepts used in this report in greater depth, we invite you to have a look at the following references [2] and [4]; or even the work of the founder of geostatistics Georges Matheron [6][7].

2 Random field

2.1 Real Random Field

Definition 2.1. Let $(\Omega, \mathcal{A}, P)$ be a probabilistic space [1] and D a domain of Ω and very often of $\mathbb{R}^d$. A random field (or a random function) on D which has values in a metric space E (very often in $\mathbb{R}$), is a two variable function denoted $Z(x;\omega)$, such that for each $x_0 \in D$, $Z(x_0;\omega)$ is a random variable on $(\Omega, \mathcal{A}, P)$ and for each $\omega_0 \in \Omega$, $Z(x,\omega_0)$ is a function of $D \to E$.

We can distinguished a studied variable $z(x)$, also known as regionalised variable, and its modelling by a random field $Z(x)$. The regionalised variable $z(x)$ is one realization of the random field $Z(x)$.

A random field is totally characterized by its finite-dimensional distributions for any value of n and any n-uplets set $x_i \in \mathbb{R}^d$, $i = 1, ..., n$:

$$F_{x_1,...,x_n}(B_1 \times ... \times B_n) = P((Z(x_1), ..., Z(x_1)) \in B_1 \times ... \times B_n),$$

where $B_1, ..., B_n$ are Borel sets of $\mathbb{R}$.

The distribution laws have to verify minimal conditions of consistency, named Kolmogorov conditions.

Definition 2.2. (Kolmogorov conditions)
We call Kolmogorov conditions the following two conditions:

1. symmetry condition: the finite-dimensional distribution law has to be constant by permutation:

$$F_{x_1,...,x_n}(B_1 \times ... \times B_n) = F_{x_{i_1},...,x_{i_n}}(B_{i_1} \times ... \times B_{i_n})$$

   where $(i_1, ..., i_n)$ is any permutation from $1, ..., n$.

2. consistency condition by the marginal:

$$F_{x_1,...,x_{n-1}}(B_1 \times ... \times B_{n-1}) = F_{x_1,...,x_n}(B_1 \times ... \times B_{n-1} \times \mathbb{R})$$

If the law of $F_{x_1,...,x_{n-1}}$ verify the Kolmogorov conditions, then there exists a random field having $F_{x_1,...,x_{n-1}}$ as finite-dimensional laws. In the following, we consider this conditions always verified.

[1] Ω is the set of system states, $\mathcal{A}$ is the events $\sigma - algebra$ which specify what can be predicted, and a probability P which attribute an apparition frequency at each system event

Definition 2.3. (Second order field)
A random field Z is said of second order if

$$Var(Z(x)) < \infty, \forall x \in D$$

Then the function

$$C(x, y) = Cov(Z(x), Z(y))$$

is named covariance function of $Z(\cdot)$. This function is well defined because $C(x, y) < (VarZ(x)VarZ(y))^{1/2} < \infty$ and symmetric. We have $C(x, x) = Var(Z(x))$.

2.2 Gaussian Random Field

Definition 2.4. $\{Y(x)\}_{x\in\Omega}$ is called a (real) Gaussian random field if $\forall n \in \mathbb{N}\backslash\{0\}, \forall x_1, ..., x_n \in \Omega$, the random vector $(Y(x_1), ..., Y(x_n))$ is Gaussian.

Remark 2.1. *$\forall x \in \Omega$, the random variable $Y(x)$ is Gaussian with mean*

$$m(x) := \mathbb{E}[Y(x)]$$

and with covariance function

$$Cov[Y(x), Y(x')] := \mathbb{E}[(Y(x) - m(x))(Y(x') - m(x'))], \ for \ x, \ x' \in \Omega.$$

2.3 Covariance function

The main property of a covariance function C is to be positive semi-definite (spd):

$$\forall n \geq 1, \forall \lambda \in \mathbb{R}^n \text{ and for all n-tuple } (x_1, ..., x_n) \text{ of } \mathbb{R}^d :$$

$$\sum_{i=1}^{n}\sum_{j=1}^{n} \lambda_i \lambda_j C(x_i, x_j) \geq 0 \tag{1}$$

This property results of the positiveness of the variance of any linear combination:

$$Var\left(\sum_{i=1}^{n} \lambda_i Z(x_i)\right) = \sum_{i=1}^{n}\sum_{j=1}^{n} \lambda_i \lambda_j C(x_i, x_j) \geq 0 \tag{2}$$

The covariance is positive definite (dp) if moreover equation (1) is strictly positive, when $\lambda \neq 0$.

Property 2.1. Here is some elementary properties of positive definite functions:

1. The class of positive definite functions is convex: Let C_1 and C_2 two positive definite functions, then $\lambda_1 C_1 + \lambda_2 C_2 \geq 0, \forall \lambda_1, \lambda_2$ is a positive definite function.
2. The class of positive definite functions is multiplicative: Let C_1 and C_2 two positive definite functions, then $C = C_1 \cdot C_2$ is a positive definite function.
3. Let $C_1, C_2, ...$ a family of positive definite functions and $\lim_{n \to +\infty} C_n(x, y) = C(x, y), \forall x, y$, then C is a positive definite function.

2.3.1 Stationarity

Definition 2.5. (Strict stationarity)
A random field $Z(\cdot)$ on $\mathbb{R}^d$ is strictly stationary if any finite-dimensional laws are invariant for any translation $h \in \mathbb{R}^d$, that is to say:

$$F_{x_1,...,x_n}(B) = F_{x_1+h,...,x_n+h}(B),$$

for any $n \in \mathbb{N}^*$, any Borel $B = B \times ... \times B_n$ of $\mathbb{R}^d$, any n-tuple $x_1, ..., x_n$ and any vector $h \in \mathbb{R}^d$.

This hypothesis is rarely verified because of its high number of verification to realize. We prefer the second order hypothesis.

Definition 2.6. (Second order stationarity/Low stationarity)
A second order random field $Z(\cdot)$ on $\mathbb{R}^d$ is second order stationary if the first two moments exist and are invariants by translation:

$$E[Z(x)] = E[Z(x + \tau)] \tag{3}$$

$$Cov(Z(x), Z(y)) = C(x, y) = Cov(Z(x + \tau), Z(y + \tau)), \tag{4}$$

for any $x, y, \tau \in \mathbb{R}^d$.

Condition (3) is equivalent to say that the first moment is constant and condition (4) is equivalent to say that covariance between $Z(x)$ and $Z(y)$ depends only of the vector $x - y = h$. Thus, we use the function $C(h)$ with $h \in \mathbb{R}^d$ as the covariance function of $Z(\cdot)$.

Definition 2.7. (Second order stationarity: usual definition)
A random field $Z(\cdot)$ on $\mathbb{R}^d$ is second order stationary if the first two moments exist and verify:

$$E(Z(x)) = \mu \tag{5}$$

$$Cov(Z(x), Z(x+h)) = C(h), \tag{6}$$

for any x and $h \in \mathbb{R}^d$.

Remark 2.2. *A 2nd order stationary Gaussian field Z is entirely determined by its mean and its covariance function $C(h)$.*

Remark 2.3. *It is important to mention that if a random field Z is stationary to the strict meaning and if $Z \in L^2$, then Z is stationary in L^2. The inverse is usually false, but the two notions coincide if Z is a gaussian random field.*

Property 2.2. The covariance function $C(h)$ of a second order stationary random field has the following properties:

1. $\forall h, x \in \mathbb{R}^d,\ |C(h)| \leq C(0) = Var(Z(x))$.
2. $\forall n \geq 1,\ \lambda \in \mathbb{R}^n$ and $x_1, x_2, ..., x_n \subseteq \mathbb{R}^d$:

$$\sum_{i=1}^{n} \sum_{j=1}^{n} \lambda_i \lambda_j C(x_i - x_j) \geq 0.$$

3. If $A : \mathbb{R}^d \longrightarrow \mathbb{R}^d$ is linear, the random field $X^A = X_{Ax},\ x \in \mathbb{R}^d$ is stationary of covariance $C^A(x) = C(Ax)$. C^A is positive definite (p.d.) if C is p.d. and A has full rank.
4. If C is continuous at the origin, then C is uniformly continuous everywhere.

Property 2.3.

If $C_1, C_2, ...$ are stationary covariances, the following functions are so :

1. $C(h) = \lambda_1 C_1(h) + \lambda_2 C_2(h)$, if $\lambda_1, \lambda_2 \geq 0$.

2. More generally, if $C(\cdot, u),\ u \in U \subseteq \mathbb{R}^k$ is a stationary covariance for each u and if μ is a positive measure on $\mathbb{R}^k$ such as $C_\mu(h) = \int_U C(h;u)\mu(du)$ exists for any h, then C_μ is a stationary covariance.
3. $C(h) = C_1(h)C_2(h)$.
4. $C(h) = \lim_{n\to\infty} C_n(h)$ once the limit exists for any h.

2.3.2 White noise

Definition 2.8. (Strict white noise)
A random field Z is a a strict white noise, if the variables $(Z(x))_{x\in\mathbb{R}^d}$ are centered, independents and identically distributed (*iid*):

$$\forall x \in \mathbb{R}^d,\ \mathbb{E}(Z(x)) = 0 \tag{7}$$
$$\forall x \in \mathbb{R}^d,\ \mathbb{E}(Z(x)^2) = \sigma^2 \tag{8}$$
$$\forall x \neq y,\ Z(x) \perp\!\!\!\perp Z(y) \tag{9}$$

Definition 2.9. (Weak white noise)
A random field Z is a a weak white noise, if the variables $(Z(x))_{x\in\mathbb{R}^d}$ are centered, uncorrelated and identically distributed (*iid*):

$$\forall x \in \mathbb{R}^d,\ \mathbb{E}(Z(x)) = 0 \tag{10}$$
$$\forall x \in \mathbb{R}^d,\ \mathbb{E}(Z(x)^2) = \sigma^2 < \infty \tag{11}$$
$$\forall x \neq y,\ Cov(Z(x), Z(y)) = 0 \tag{12}$$

Remark 2.4. *A strict white noise is strictly stationary process. A weak white noise is stationary process in L^2 (second order stationary process - FAST2). Moreover, a strict white noise to the second order is a weak white noise.*

2.3.3 Isotropy

A covariance function $C(h)$ is said isotrope if it depends only on the distance $r = \|h\|$ and not the direction of the vector h. We will therefore note $C(h) = C(\|h\|) = C(r)$.

Theorem 2.1. (Schoenberg, 1938)
A function $C(r)$ is an isotropic covariance function in $\mathbb{R}^d$ for any d, if and only if $C(r)$ is in the form

$$C(r) = \int_0^\infty exp(-r^2/t^2)\nu(dt) \tag{13}$$

where ν is a bounded positive measure on $\mathbb{R}^+$.

2.4 Variogram

In the literature, we find the expression "variogram" and "semivariogram". Some authors [6] consider that we must use the term of semivariogram for $\gamma(h)$ as defined by $\gamma(h) = C(0) - C(h)$, the variogram correspond to $2\gamma(h)$. This is the choice that we made in this report.

2.4.1 Variogram of a stationary second order random field

Definition 2.10. (A first definition)
Let $Z(x)$ a stationary second order random field on $\mathbb{R}^d$. The variogram of $Z(x)$ is the function

$$\gamma(h) = \frac{1}{2}E[(Z(x+h) - Z(x))^2] = \frac{1}{2}Var\{Z(x+h) - Z(x)\} \tag{14}$$

Property 2.4. (Variogram properties)

1. $\gamma(h) \geq 0,\ \gamma(-h) = \gamma(h)$ *and* $\gamma(0) = 0$.
2. $\gamma(h) = C(0) - C(h)$, because

$$\begin{aligned}
\gamma(h) &= \frac{1}{2}E[(Z(x+h) - Z(x))^2] \\
&= \frac{1}{2}E[Z(x+h)^2 - 2Z(x+h)Z(x) + Z(x)^2] \\
&= \frac{1}{2}[Var(Z(x+h)) - 2Cov(Z(x+h), Z(x)) + Var(Z(x))] \\
&= \frac{1}{2}[2C(0) - 2C(h)] \\
&= C(0) - C(h)
\end{aligned}$$

3. A variogram is conditionally negatively definite: $\forall \lambda \in \mathbb{R}^n$ such as $\sum_{i=1}^n \lambda_i = 0$, then:

$$\forall \{x_1, x_2, ..., x_n\} \subseteq \mathbb{R}^d, \ \sum_{i=1}^{n} \sum_{j=1}^{n} \lambda_i \lambda_j \gamma(x_i - x_j) \leq 0.$$

4. If A is linear transformation on $\mathbb{R}^d$, $h \mapsto \gamma(Ah)$ is a variogram if γ is so.
5. The properties 5-(a,b,d) of a covariance function (cf. Prop. 2.2) are used for the variogram.
6. If γ is continuous at 0, then γ is continuous for any x where γ is localy bounded.
7. If γ is bounded next to 0, $\exists a$ and $b \geq 0$ such as $\forall h, \ \gamma(h) \leq a\|h\|^2 + b$.

2.4.2 Intrinsic hypothesis

As we have seen before ((14)), the variogram is not directly defined by its values of $Z(x)$, but rather by $Z(x+h) - Z(x)$. The second order hypothesis, which suppose the existence of the first two moments of $Z(x)$, is therefore restrictive if we decided to use only the variogram (and not the covariance function).

It is also useful to define lower stationarity hypothesis, or named intrinsic stationarity hypothesis.

Definition 2.11. (Usual definition of the variogram)
Let $Z(x)$ a random field on $\mathbb{R}^d$. $Z(x)$ verify the intrinsic hypothesis if:

$$E[Z(x) - Z(x+h)] = \langle a, h \rangle \text{ et } \frac{1}{2} Var(Z(x+h) - Z(x)) = \gamma(h), \qquad (15)$$

$\forall x, \forall h \in \mathbb{R}^d$. $\langle a, h \rangle$ is also named as a linear trend of $Z(x)$. If the linear trend is null ($a = 0$), then the intrinsic hypothesis are reformulated as follows:

$$\left\{ \begin{array}{rcl} E[Z(x) - Z(x+h)] & = & 0 \\ \frac{1}{2} E[(Z(x+h) - Z(x))^2] & = & \gamma(h) \end{array} \right. \qquad (16)$$

It is important to notify that the second order stationarity hypothesis is stronger and entails the intrinsic hypothesis. However, the opposite is false, because the intrinsic hypothesis don't make hypothesis on the moments of $Z(\cdot)$, but only on the existence of the moments for the increments [2].

Thus, the class of random fields which verify the intrinsic hypothesis is larger than the class of random fields which verify the second order stationarity hypothesis.

Moreover, if any covariance function can be written in the form a variogram with $\gamma(h) = C(0) - C(h)$, the opposite is false in general. To switch from a variogram to a covariance function is only possible under the second order stationarity hypothesis.

Proposition 2.1. *If a random field $Z(x)$ verifying the intrinsic hypothesis has a bounded variogram*

$$\lim_{\|h\|\to\infty} \gamma(h) = \gamma(\infty) < \infty, \tag{17}$$

Then $Z(x)$ is a second order stationary random field.

2.4.3 Continuity and differentiability

Definition 2.12. (Continuity)
The random field $Z(x)$ is said to be continuous in the mean square (continuous quadratic mean), if:

$$\mathbb{E}([Z(x+h) - Z(x)]^2) \longrightarrow 0, \text{ when } \|h\| \to 0.$$

This condition is satisfied if and only if the variogram $\gamma(h)$ is continuous at h=0, that is to say if there is no nugget effect.

In other words, an intrinsic random field is continuous in quadratic mean if its variogram γ is continuous at h=0. In this case, the variogram γ is continuous on any set where γ is bounded. Thus, a second order stationary random field is continuous in quadratic mean if its covariance C is continuous at h=0. In this case, the covariance C is continuous everywhere (cf. Prop. 2.2).

[2] For instance, Yaglom (1987) talks about stationarity hypothesis of increments when he mentions the intrinsic hypothesis.

More precisely, if a random field admits a continuous variogram everywhere except the origin, then this field is the sum of two non-correlated fields, one associated to a pure nugget effect, and the other with a continuous variogram everywhere.

Definition 2.13. (Differentiability)
The random field $Z(x)$ is said to be differentiable in the mean square on $\mathbb{R}$ if the second derivative γ'' exists everywhere et Z is stationary of covariance γ''. If $m \in \mathbb{N}*$, we will say that Z is differentiable in mean square to the order m if $Z^{(m-1)}$ exists in the mean square and if $Z^{(m-1)}$ is differentiable in the mean square.

Let Z be stationary with covariance C, then Z is differentiable to the order m if $C^{(2m)}(0)$ exists and is finite. In this case, $Z^{(m)}$ is stationary with the covariance $t \mapsto (-1)^m C^{(2m)}(t)$.

2.4.4 Graphical representation of a variogram

There exist two types of variogram: the bounded variograms and the unbounded variograms.

Bounded variograms
Thanks to the Proposition 2.1. we know that when the variogram is bounded, it corresponds to a covariance function $C(h) = \gamma(\infty) - \gamma(h)$. Thus we retrieve the main characteristics of the covariance functions:

- The value $\gamma(\infty) = lim_{\|h\| \to \infty} \gamma(h)$ is equal to the variance of the field: it is called the sill of the variogram.
- The continuity of $\gamma(h)$ in $h = 0$ is linked to the regularity of the random field. The jump of discontinuity at the origin of the variogram is the nugget effect.
- The range is the distance where the variogram reaches the sill, either exactly (true range) or asymptotically (practical range).

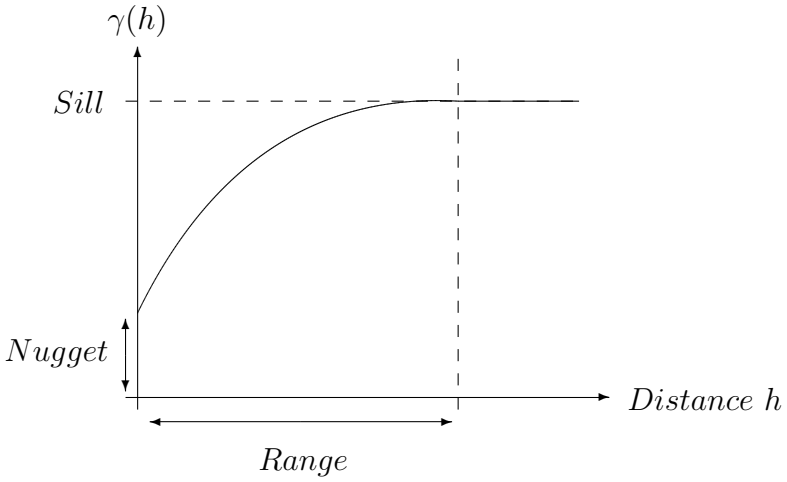

Figure 1: Theoretical semivariogram

2.4.5 Variogram behavior near the origin

The continuity and the regularity in the space of the random field $Z(x)$ are translated in the variogram behavior near the origin. We can roughly separate in decreasing order of regularity four types of behavior near the origin :

- (a) Parabolic trend: the variogram $\gamma(h)$ is twice differential at h=0. Thus, $Z(x)$ is itself differentiable (its mean square converge). Consequently, $Z(x)$ presents a high degree of regularity.
- (b) Linear behavior (oblique tangent at the origin): the variogram $\gamma(h)$ is continuous at the origin h=0 but not differential. Thus, $Z(x)$ is continuous in the mean square but not differentiable. Consequently, $Z(x)$ is less regular.
- (c) Nugget effect: The variogram $\gamma(h)$ does not approach 0 when h approaches 0, so it is discontinuous at the origin. Thus, $Z(x)$ is not even continuous in the mean square. Consequently, $Z(x)$ is highly irregular.
- (d) Completely random limiting case: For any distinct points x and x', $Z(x)$ and $Z(x')$ are independent regardless how close they are. It is also called pure nugget effect or white noise.

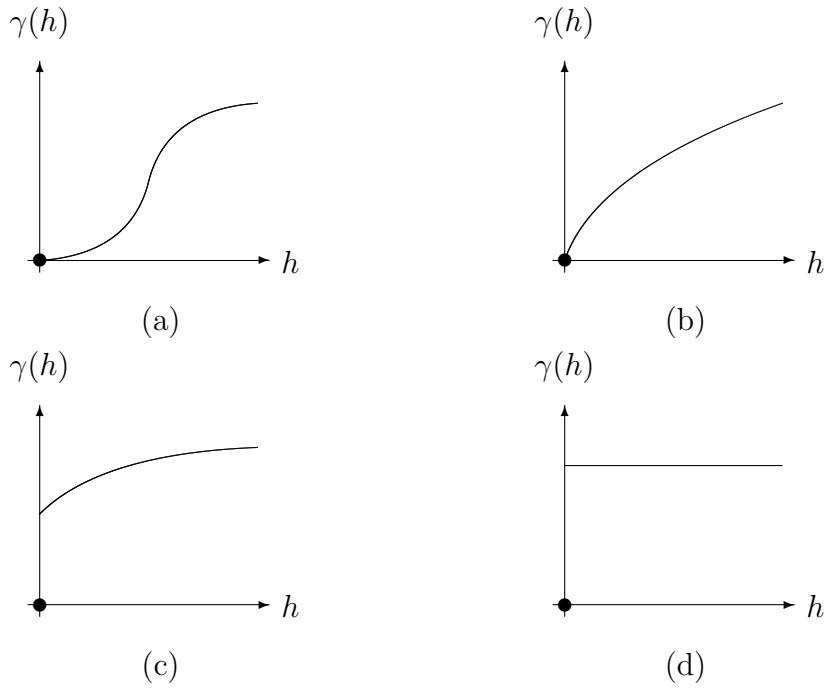

Figure 2: Variogram behavior near the origin

2.4.6 Anisotropy

There is anisotropy when the variogram is not the same in all the directions of the space. In contrary, in the isotropic case, the variogram depends only on the distance norm. We said that there is geometric anisotropy when simple linear transformation of the coordinates is enough to restore isotropy (thus the sill is the same in any directions). In other words, a variogram γ on $\mathbb{R}^d$ present a geometric anisotropy if it results of an A-linear deformation of an isotropic variogram γ_0 :

$$\gamma(h) = \gamma_0(\|Ah\|).$$

This variogram has the same level of still in any directions, but the range differs depending on the directions.

Moreover, there is other cases of anisotropy, such as zonal anisotropy (also know as stratified anisotropy) where the sill is not the same in all the directions.

2.4.7 Examples of covariances and variograms

The following examples in Table 1 are some isotropic variograms on $\mathbb{R}^d$ mainly used in geostatistics. The first five variograms, associated with a stationary covariance $C(h) = C(0) - \gamma(h)$, are bounded, with two parameters: the range $a > 0$ and the sill $\sigma^2 > 0$. Recall that $\|\cdot\|$ is the euclidean norm on $\mathbb{R}^d$.

In the simulation part of this report, we use only the first four covariance functions. To get more information on the other covariance functions, such as Matérn and Power, we invite you to look at C.E. Rasmussen (2006) [9].

Table 1: Examples of covariance functions

Name	**Function**
Pure nugget	$\gamma(h;\sigma^2) = \begin{cases} \sigma^2 & ,\text{if } h > 0. \\ 0 & ,\text{if } h = 0. \end{cases}$
Exponential	$\gamma(h;a,\sigma^2) = \sigma^2(1 - exp(-\|h\|/a))$
Spherical	$\gamma(h;a,\sigma^2) = \begin{cases} \sigma^2(\frac{3}{2}\|h\|/a - \frac{1}{2}(\|h\|/a)^3) & ,\text{if } \|h\| \leq a. \\ \sigma^2 & ,\text{if } \|h\| > a. \end{cases}$
Gaussian	$\gamma(h;a,\sigma^2) = \sigma^2(1 - exp(-(\|h\|/a)^2))$
Matérn	$\gamma(h;a,\sigma^2,\nu) = \sigma^2(1 - \frac{2^{1-\nu}}{\Gamma(\nu)}(\|h\|/a)^\nu \mathcal{K}_\nu(\|h\|/a))$ [3]
Power	$\gamma(h;b,c) = b\|h\|^c$, for $0 < c \leq 2$

Adding to the Table 1, there exists combined models, named "trundle models", using different covariance functions. Indeed, each of the previous models can be used separately, but we can also add them up with different sills, ranges and eventually anisotropy.

[3] Where $\mathcal{K}_\nu(\cdot)$ is the modified Bessel function of parameters $\nu > -1$[2; 227; 200].

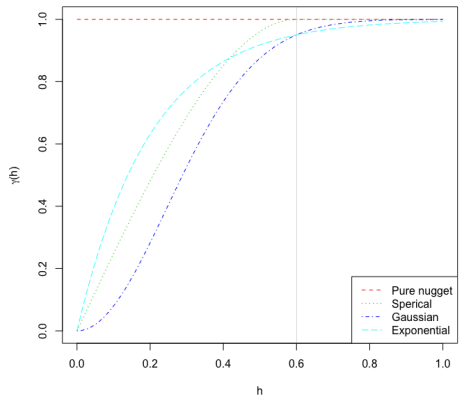

Figure 3: Theoretical variograms for the real range of the spherical variogram and the practical range of the exponential and gaussian variograms; with nugget = 0, sill = 1 and range = 0.6.

On the Figure 3, we drew the curves of the three most common theoretical variogram models that are: spherical (green), exponential (light blue) and Gaussian (dark blue) with the same variogram parameters (nugget = 0, sill = 1 and range = 0.6). We can see that there are two kinds of range depending on the covariance behavior. In fact, as shown in the Figure 3 the range is not equal if it is a covariance which converge asymptotically or directly to the sill. Here, the spherical covariance has a real range, while the exponential and gaussian covariance has a practical range. The practical range drawn is by definition the lag at which 95% of the sill is exceeded. To get the Figure 3, we calculated the effective range in order to compare graphically different models which have the same range more easier:

Gaussian model:

$$
\begin{aligned}
0.95 &= 1 - exp(-(0.6/a)^2) \\
\iff & \; exp(-(0.6/a)^2) = 0.05 \\
\iff & \; a = \sqrt{-0.36/ln(0.05)} \\
& (\text{car } a > 0) \\
& \Rightarrow a \approx 0.346657
\end{aligned}
$$

Exponential model:

$$
\begin{aligned}
0.95 &= 1 - exp(-0.6/a) \\
\iff & \; exp(-0.6/a) = 0.05 \\
\iff & \; a = -0.6/ln(0.05) \\
& \Rightarrow a \approx 0.200228
\end{aligned}
$$

Thus, we obtain the same effective range for the two theoretical variogram

models (exponential and gaussian) and equal to the real range of the spherical model.

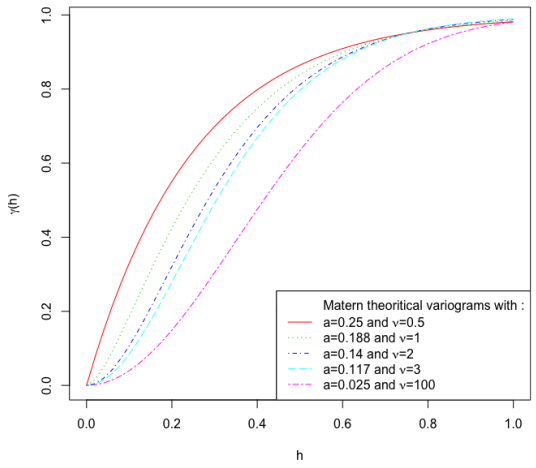

Figure 4: Matérn theoretical variogram with different ranges and ν.

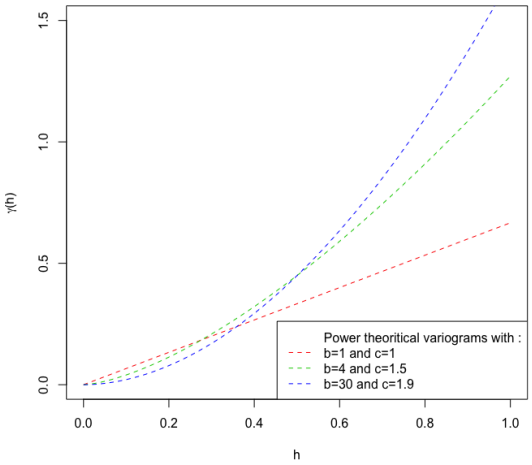

Figure 5: Power theoretical variogram with parameters b and c.

The Figure 4 represents several graphics of the Matérn variogram function. In the Matérn covariance, the interesting parameter is ν. ν controls the regularity at the origin. It is really important because the regularity in 0 for the variogram causes the regularity of $Z(\cdot)$ in quadratic mean. Therefore, the biggest ν is, the more regular in 0 γ is, and so the more $Z(\cdot)$ is regular. We observe that $\nu = 0.5$ is the exponential variogram, continuous but not differentiable in 0. Moreover, $\nu = \infty$ corresponds to the gaussian variogram which is $\mathcal{C}^\infty$ and consequently $Z(\cdot)$ is also indefinitely differentiable.

The Figure 5 represents several graphics of the Power variogram function. The main feature of the power variogram is to be unbounded. It has no range and sill. The Power variogram is a particular variogram because it is invariant by scale change: $\forall s > 0,\ \gamma(sh) = s^c\gamma(h)$. We call this kind of function self-similar. We associate it to a spatial phenomenon without scale and it is the only one among the model of Table 1.

3 Simulations

In order to simulate a random field, there exist conditional and non-conditional approach. A non-conditional method does not take into account any information to simulate a random field. The conditional methods are based on the fact that we already know the values of the simulation at some points.

3.1 LU and Cholesky decompositions

The Lower-Upper (LU) decomposition is a method consisting in a matrix decomposition as the product of a lower triangular matrix and an upper triangular matrix. The Cholesky decomposition is based on the decomposition of a positive defined and symmetric matrix. This decomposition is very useful in our case, because we decompose covariance matrices that are by definition symmetric positive definite matrices.

Theorem 3.1. (Cholesky Decomposition) Let $A \in \mathcal{S}_n^{++}(\mathbb{R})$. There exists a unique upper triangular matrix $T \in \mathcal{M}_n(\mathbb{R})$ with strictly positives diagonals coefficients such as $A = T^T T$.

To demonstrate this theorem, we consider two Lemmas.

Lemma 3.1. Any positive definite symmetric real matrix is the Gram matrix of a vector family. In other words, any positive symmetrical real square matrix A can be written as: $A = B^T B$, where B is a (non-unique) real square matrix and $rg(B) = rg(A)$.

Lemma 3.2. (Factorization) Let $A \in \mathcal{S}_n^{++}(\mathbb{R})$. There exists upper triangular matrix T and an orthogonal matrix Q such as:

$$A = QT.$$

Proof. **Existence:** If A is a positive definite real symmetric matrix, then: $A = B^T B$ and $B = QT$. Hence, $A = (QT)^T QT = T^T Q^T QT$ and as Q is an orthogonal matrix $Q^T = Q^{-1}$. Thus, $A = T^T T$.

Uniqueness: Let $S \in \mathcal{M}_n(\mathbb{R})$ another upper triangular matrix with strictly positive diagonal coefficients such that $A = S^T S$. Then $ST^{-1} = (TS^{-1})^T$ and $(S^{-1})^T$ is an upper triangular matrix and T^T is a lower triangular matrix. So

ST^{-1} is a diagonal matrix. Moreover, $(ST^{-1})^{-1} = TS^{-1} = (TS^{-1})^T = ST^{-1}$, and all the diagonal coefficients of ST^{-1} are strictly positive. Consequently, the diagonal coefficients of ST^{-1} are equal to 1, that is to say $S = T$. □

Remark 3.1. *The converse is true: if $A \in \mathcal{M}_n(\mathbb{R})$ and if there exists a superior triangular matrix with strictly positives diagonals coefficients $T \in \mathcal{M}_n(\mathbb{R})$ such as $A = T^T T$, then $A \in \mathcal{S}_n^{++}(\mathbb{R})$.*

Algorithm of the Cholesky decomposition

Note $A = (a_{i,j})_{1 \leq i,j \leq n}$ and $T = (t_{i,j})_{1 \leq i,j \leq n}$ ($t_{i,j} = 0$ *if* $i > j$). For all $i, j \in \{1, ...n\}$,

$$a_{i,j} = \sum_{k=1}^{min(i,j)} t_{k,i} t_{k,j}.$$

Step 1. We have $a_{1,1} = t_{1,1}^2$ hence $t_{1,1} = \sqrt{a_{1,1}}$. Then, for $j \in \{2, ..., n\}$, we have $a_{1,j} = t_{1,1} t_{1,j}$ and so $t_{1,j} = \frac{a_{1,j}}{t_{1,1}}$.

Step i, $2 \leq i \leq n$**.** In step i, we suppose that we calculated all the coefficients $t_{i',j}$ for $i' < i$. We have $a_{i,i} = \sum_{k=1}^{i} t_{k,i}^2$. Then for $j \in \{i+1, ..., n\}$, we have $a_{i,j} = \sum_{k=1}^{i} t_{k,i} t_{k,j}$ and so $t_{i,j} = \frac{1}{t_{i,i}}(a_{i,j} - \sum_{k=1}^{i-1} t_{k,i} t_{k,j})$

This method is applied when we are in the case of a limited number of points. Indeed when A dimension is to big, the computation time becomes quickly quite long.

Remark 3.2. *The total cost of calculating the Cholesky decomposition, as a number of elementary arithmetic operations, is $\frac{1}{3}n^3 + O(n^2)$.*

3.1.1 Non conditional simulations

Suppose we have n points to simulate with covariance C(h). Let $K_{n \times n}$ be the covariance matrix. We decompose this matrix as $K_{n \times n} = LU$, with $L = {}^tU$. We draw n independant random values $y_i, i = 1...n$ with distribution $\mathcal{N}(0, 1)$. Set z=Ly; z is then a realization of Z having the right covariogram.

Proof. $Cov[LY, LY] = \mathbb{E}[LY^t Y^t L] = L\mathbb{E}[Y^t Y]^t L = L^t L = LU = K_{n \times n}$ □

3.1.2 Conditional simulations

The approach is very similar to the previous case. Let N conditional points and n points to simulate. We place in a vector the N conditioning points followed by the n points to simulate. The matrix $K_{(N+n)\times(N+n)}$ is decomposed as before in LU.

We partition L into 4 separate blocks:

$$L = \begin{pmatrix} L_{11} & 0 \\ L_{21} & L_{22} \end{pmatrix}$$

The block L_{11} corresponds to the conditioning points, the block L_{12} to the points to be simulated, the block L_{21} put in relation the points to simulate and the conditioning points.

A vector $y_{(N+n)}$ of $\mathcal{N}(0,1)$ is formed. We then have:

$$\begin{pmatrix} Z_1 \\ Z_2 \end{pmatrix} = \begin{pmatrix} L_{11} & 0 \\ L_{21} & L_{22} \end{pmatrix} \begin{pmatrix} Y_1 \\ Y_2 \end{pmatrix}$$

We get :

$$Z_1 = L_{11}Y_1$$

$$Z_2 = L_{21}Y_1 + L_{22}Y_2$$

$Z_1 = z_1$ was observed. We must therefore impose $y_1 = L_{11}^{-1}Z_1$. Knowing y_1, all you have to do is randomly draw n values of a $\mathcal{N}(0,1)$ to form y_2 and then calculate z_2 using the expression above (note that $L_{21}y_1$ is constant and does not need to be recalculated for each new realization).

Remark 3.3. *This simulation method is extremely efficient and fast because a single matrix inversion is required. Additional realizations can be obtained easily at very low cost. The main limitation is one of memory. Indeed, (N + n) can not exceed a few thousand because then the K matrix becomes too wide and can not be stored in memory.*

Remark 3.4. *K must be non singular in order to do the decomposition of Cholesky. this implies that a point to simulate cannot coincide with an observed point.*

3.1.3 Practical application of the Cholesky decomposition

The following simulations are realizations on a regular grid 51×51 on $[0, 200]^2$ of a centered gaussian process with different covariances. In our simulations, our main objective was to compare the different gaussian random fields. In order to do this, we took the same settings: sill (=1), nugget (=0) and range (real and practical = 20). The random part of the Cholesky method comes from the multiplication of the decomposed matrix with a standard Gaussian random sample. Only this Gaussian sample is created randomly. Thus, we selected the randomness with `set.seed()` function in the computer software R.

Firstly we got, for each of the gaussian random fields which have different covariance functions, the same histogram of the value of $Z(\cdot)$ in accordance with the Figure 6. This histogram shows us that the distribution keeps effectively a (perfect in this case) gaussian distribution of average 0.

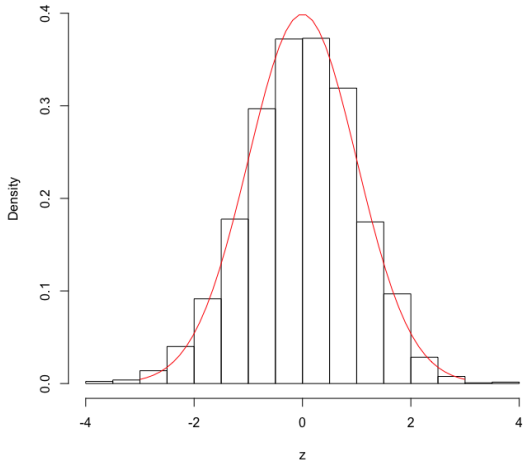

Figure 6: Histogram of $Z(\cdot)$

The Figure 7 represents a pure nugget effect. This case comes from a weak white noise. The pure nugget effect is due to the fact that the covariance is null between a point and all the other points distant from h. Thus, the gaussian values are chosen totally randomly whatever the distance h as we can see on Figure 7-a. Therefore, the variogram of the Figure 7-b of function

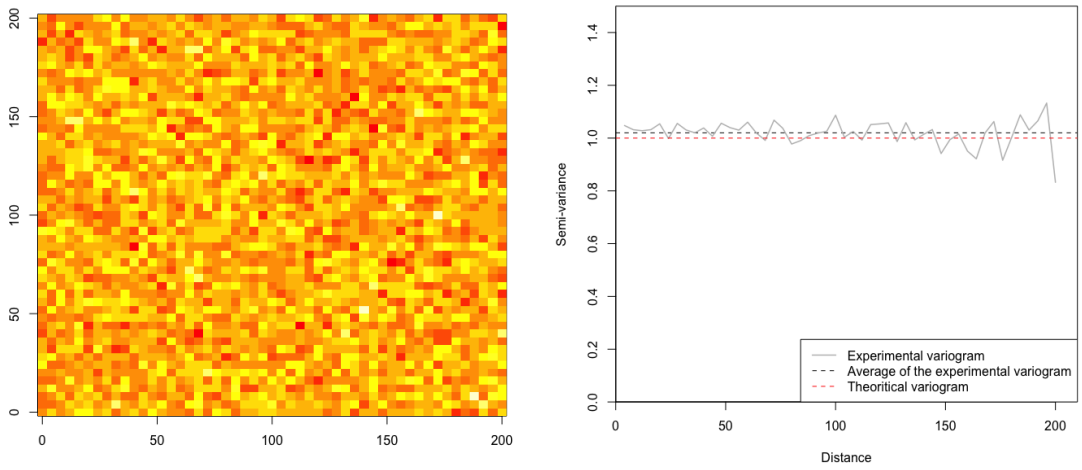

(a) (b)

Figure 7: Pure nugget effect (a) gaussian random field and (b) variogram with sill = 1.

$\gamma(h) = C(0) - C(h)$ (with $C(\cdot)$ the covariance function) is equal to 0 for $h = 0$ and around 1 for $h > 0$.

On the Figure 8-a, we already observe a relative order graphically in the gaussian random field of spherical covariance. The aspect of random field is very granular, that is to say that the red points are not aggregate due to the regularity of the covariance in the origin. Indeed, the spherical covariance is continuous but not differential in h=0. Furthermore, the variogram on Figure 8-b really shows a spherical covariance, as it should be the case with the dashed red line. We can see some variations around the theoretical variogram due to the fact that a random field is a stochastic process (the random part).

The Figure 9-a represents a gaussian random field of exponential covariance with a range equal to 20. The field is almost the same that the one with the spherical covariance. This due to the behavior of the curve at h=0.

The Figure 10-a represents a gaussian random field of gaussian covariance with a range equal to 20. For matrix calculation reasons of the Cholesky decomposition, we couldn't go higher in term of range. In fact the gaussian covariance (sill=1) is $C(h) = exp(-(\|h\|/a)^2)$. Thus, when the distance h is

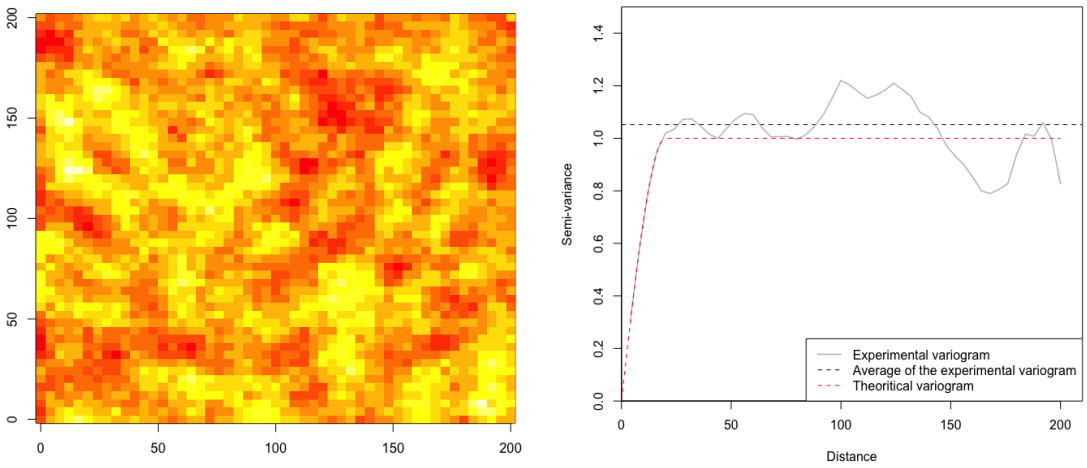

(a) (b)

Figure 8: (a) Gaussian random field and (b) variogram of spherical covariance with nugget = 0, sill = 1 and range = 20.

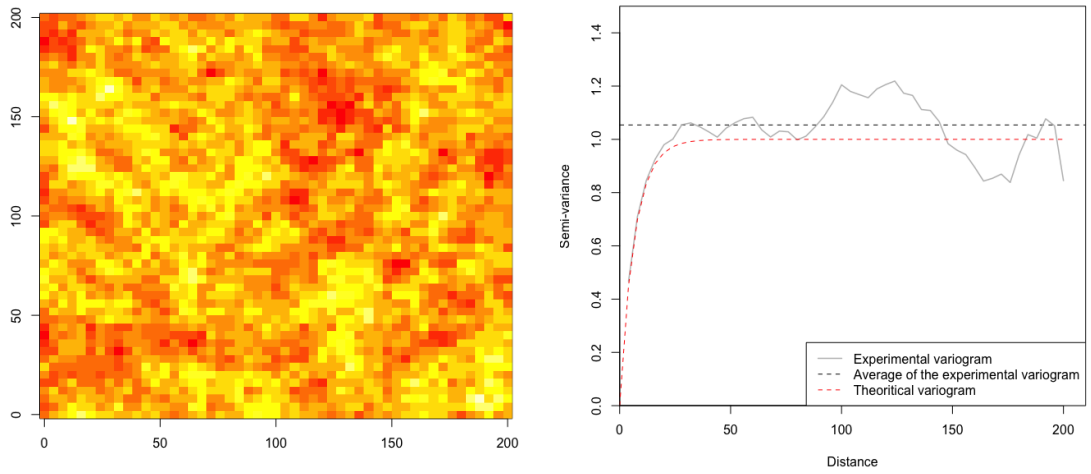

(a) (b)

Figure 9: (a) Gaussian random field and (b) variogram of exponential covariance with nugget = 0, sill = 1 and range = 20.

smaller than the range a and far from a, in our case that is to say close to 1, the covariance is approximately the same for any neighboring h. For instance, let suppose we have a range of 120: $C(1) \approx 0.9999306$ and $C(2) \approx 0.9997223$ so $C(1) \approx C(2)$. Thus, the Cholesky decomposition algorithm can't work if the range is to higher, because the matrix becomes a singular matrix. This particular case is also a real problem in the Cholesky decomposition.

Furthermore, the Figure 10-a is different from the previous fields. The aspect is a blurred copy of the exponential or the spherical covariance (which are similar). In fact, it is still the regularity at the origin which causes the aspect. Indeed, the gaussian covariance is continuous and indefinitely differentiable at the origin: the gaussian model present a high degree of regularity. We observe on the Figure 10-b that the experimental variogram is really a gaussian variogram mainly because it has the particular shape at the origin.

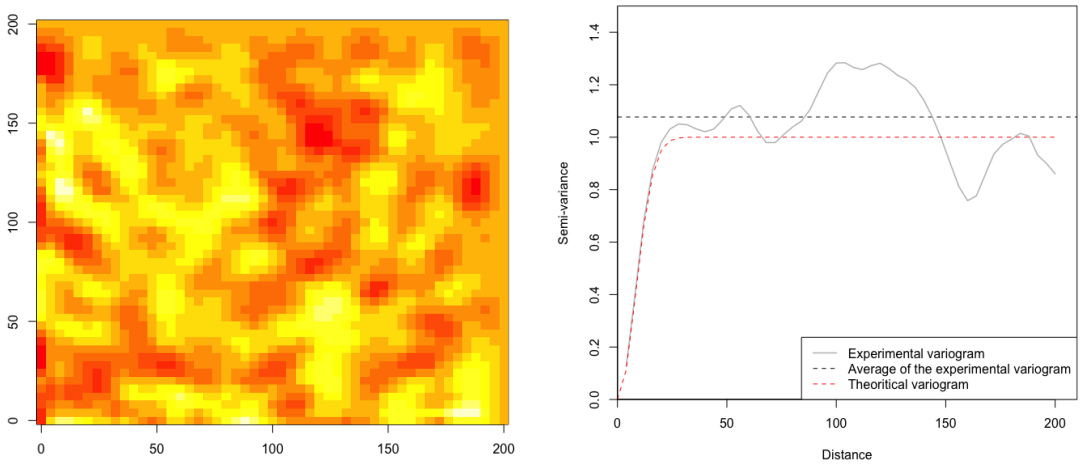

(a) (b)

Figure 10: (a) Gaussian random field and (b) variogram of gaussian covariance with nugget = 0, sill = 1 and range = 20.

Though this simulations, we note that the variograms have the same shape due to the fixed randomness and the differences come from the covariance function which smooth the variogram out or break it up.

In order to compare the calculation time of each method (Cholesky decomposition and turning bands), we used the function `proc.time()` which gave us more tools to compare finally the performance of the methods to simulation a gaussian random field of exponential covariance. For the Cholesky decomposition, the elapsed time is 3.070 seconds which is quite long.

3.1.4 Empirical convergence of the experimental variograms

The Figure 11 is a simulation of variograms for 3 different ranges (28, 80 and 160) of 20 gaussian random fields each time with an exponential covariance. Through this simulations, we traced the theoretical variograms, the average of the 20 experimental variograms and the confidence interval of them. We observe already with only 20 fields that the experimental variograms converge empirically (in average) to the theoretical variogram. Moreover, we see that the confident interval is closer to the average variogram when the range is small compared to the dimension of the field.

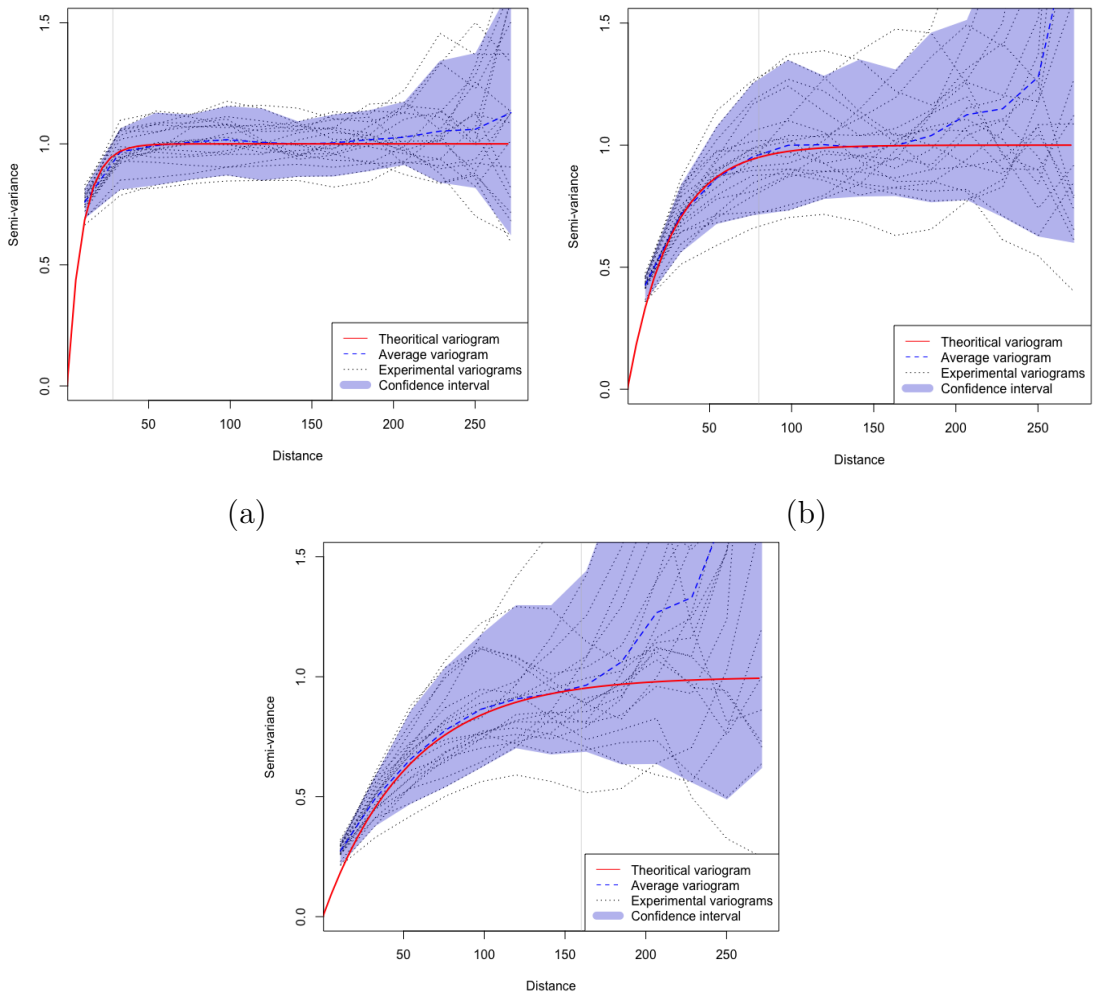

Figure 11: Averages of 20 exponential variograms with three practical ranges: (a) 28, (b) 80 and (c) 160.

3.2 Spectral method

The main problem of the Cholesky decomposition is that we have inevitably to stay in a small dimension field due to the matrix calculations. To solve this problem, the spectral method focuses on the covariance function.

The two following methods (spectral and turning bands) are applied when we are in the case of any number of points.

3.2.1 Fourier transform of a measure

Definition 3.1. Let μ be a finite measure on $(\mathbb{R}^d, Bor(\mathbb{R}^d))$. We call Fourier transform of μ, the function $\hat{\mu} : \mathbb{R}^d \longrightarrow \mathbb{C}$, defined by:

$$\forall t \in \mathbb{R}^d,\ \hat{\mu}(t) := \int_{\mathbb{R}^d} exp(i\langle t, x\rangle) d\mu(x) \tag{18}$$

When μ is the law of a random vector, $\hat{\mu}$ is the characteristic function of X.

$$\text{If } \mu = P_X,\ \hat{\mu}(t) = \varphi_X(t) = \mathbb{E}(e^{i\langle t, X\rangle}) \tag{19}$$

Definition 3.2. A property P takes place *μ-almost everywhere* in X, if there exists $Z \in \mathcal{M}$ such as $\mu(Z) = 0$ and such as P takes place for any $x \in X \backslash Z$.

We said also that P takes place for *μ-almost* any $x \in X$.

Theorem 3.2. (Theorem of continuity under the integral)
Let $f : (t, x) \longrightarrow f(t, x)$ a function of $I \times E$ in $\mathbb{C}$ (where I is an interval of $\mathbb{R}$). We suppose that:

- **(Measurability)** For any $t \in I$, $x \mapsto f(t, x)$ is measurable ;
- **(Continuity)** For *μ-almost* any $x \in E$, $t \mapsto f(t, x)$ is continuous on I.
- **(Domination)** There exists a function $\varphi : E \to \mathbb{R}_+$ measurable such as $\int \varphi\ d(\mu) < \infty$ and for any $t \in I$, for *μ-almost* any $x \in E$, $|f(t, x)| \leq \varphi(x)$.

Then the function

$$F : t \mapsto F(t) = \int f(t, x)\ d\mu(x) \tag{20}$$

is well defined for any $t \in I$, and is continuous on I.

Property 3.1. The Fourier transform $\hat{\mu}$ of a finite measure μ is a continuous and bounded function on $\mathbb{R}^d$. We have:

$$\forall t \in \mathbb{R}^d,\ |\hat{\mu}(t)| \leq \mu(\mathbb{R}^d) = \hat{\mu}(0). \tag{21}$$

Proof.
$|\hat{\mu}(t)| = |\int_{\mathbb{R}^d} e^{i\langle t,X\rangle} d\mu(x)| \leq \int_{\mathbb{R}^d} |e^{i\langle t,X\rangle}| d\mu(x) = \int_{\mathbb{R}^d} d\mu(x) = \mu(\mathbb{R}^d) < +\infty$.
So μ is a bounded function. The continuity is an immediate application of the theorem of continuity.

3.2.2 Spectral analysis and Bochner theorem

To introduce spectral representation of random fields, it is easier to work on complex fields $Z(x) = U(x) + iV(x)$ with $U(x)$ and $V(x)$ real random fields on $\mathbb{R}^d$.

Let $U(x)$ and $V(x)$ second order stationary random fields. In this case, $Z(x)$ is a second order stationary complex random field.

We define covariance function of $Z(x)$: $K(h) : \mathbb{R}^d \longrightarrow \mathbb{C}$:

$$\begin{aligned} K(h) &= Cov((Z(x+h), \overline{Z(x)}) \\ &= Cov(U(x+h), U(x)) + Cov(V(x+h), V(x)) \\ &+ i[cov(V(x+h), U(x)) - Cov(U(x+h), V(x))], \end{aligned}$$

with $K(-h) = \overline{K(h)}$. This function K has to be positive definite.

Definition 3.3. A positive definite function is a function $K : \mathbb{R}^d \longrightarrow \mathbb{C}$ verifying:

$$\forall n \in \mathbb{N}^*, \forall x_1, ..., x_n \in \mathbb{R}^d, \forall \lambda_1, ..., \lambda_n \in \mathbb{C}^d, \sum_{i,j=1}^{n} \lambda_i \overline{\lambda_j} K(x_i - x_j) \geq 0$$

Property 3.2. Any covariance function K is positive definite, continuing on $\mathbb{R}^d$ and verify $K(0) = 1$.

Theorem 3.3. (Bochner theorem)
Let $K : \mathbb{R}^d \longrightarrow \mathbb{C}$ a positive definite function continuous at the origin and such as $K(0) = 1$. Then, a probability measure μ on $\mathbb{R}^d$ such as $K = \hat{\mu}$. In other words, the characteristic functions coincide with the Fourier transform of the probability measures on $\mathbb{R}^d$.

In other words, a complex function $K(h)$ on $\mathbb{R}^d$ is the covariance function of a second order stationary random field complex continues in root mean square on $\mathbb{R}^d$ if and only if:

$$K(h) = \int_{\mathbb{R}^d} exp(i < \omega, h >) F(d\omega) \tag{22}$$

where $< a, b >$ is the scalar product of a and $b \in \mathbb{R}^d$, and where $F(d\omega)$ is a finite measure on $\mathbb{R}^d$, such as $\int_{\mathbb{R}^d} F(d\omega) = K(0) < \infty$.

3.2.3 Spectral method algorithm

According to the Bochner theorem, if V is a random vector of the law of F, and if U is a uniform variable on $[0, 1]$, then the random function defined by:

$$Y(x) = \sqrt{2}\ cos(\langle V, x\rangle + 2\pi U),\ x \in \mathbb{R}^d \tag{23}$$

is a second order stationary random function (named FAST2) and reduced centered function of covariance function K.

Indeed, we know that

$$\int_0^1 cos(\langle V, x\rangle + 2\pi u) du = 0$$

thus

$$E(Y) = E(E(Y|V)) = 0$$

and

$$\begin{aligned} C(h) &= 2 \int_{\mathbb{R}^d} \int_0^1 cos(\langle v, x\rangle + 2\pi u) cos(\langle v, (x + h)\rangle + 2\pi u) du\ F(dv) \\ &= \int_{\mathbb{R}^d} cos(\langle v, h\rangle) F(dv) \end{aligned}$$

Therefore Y is a centered field of covariance $C(\cdot)$. This suggests the following algorithm.

Spectral method:

1. Generate n vectors $v_1, ..., v_n \sim F$ and n values $u_1, ..., u_n \sim \mathcal{U}$ independents.
2. For any $x \in \mathbb{R}^d$, we calculate:

$$Y(x) = \sqrt{\frac{2}{n}} \sum_{i=1}^{n} cos(\langle v_i, x \rangle + 2\pi u_i).$$

The main problem of the spectral method is its asset: the Fourier transform change the properties at the origin which is the point which defined the regularity of the field. The covariance functions less regular at the origin like spherical or exponential have a more scattered spectral measure. The spectral method is thus less efficient. To solve this problem, Matheron [8] proposed the turning bands method.

3.3 The Turning Bands method

In this method we will represent a random variable in three dimensions by a linear combination of random variables simulated on lines where each line is simulated independently of the others.

It is assumed that the field to be simulated is second-order stationary and isotropic.

We denote $C_s(r)$ the covariance of the field we want to simulate. The subscript s represents the term "simulated".

We choose an arbitrary origin 0 in $\mathbb{R}^3$ and generate L lines i such that the corresponding direction vectors u_i are uniformly distributed on the unit sphere.

Let x_k be the points to be simulated where $k \in \{1, ..., N\}$. We denote $x_{ki} = x_k \cdot u_i$ the projection of the point x_k on the line i.

Along each line i, we generate a second-order stationary unidimensional discrete process having zero mean and covariance function $C_1(\xi)$, where ξ is the coordinate on line i. We will derive later the correspondence between $C_1(\xi)$ and the covariance function of the field.

Then at every point x_k of the field, there are L assigned values $z_i(x_{ki})$, where $i = 1, ..., L$, from the unidimensional realizations. Finally, assign to the point x_k the value $z_s(x_k)$ given by

$$z_s(x_k) = \frac{1}{\sqrt{L}} \sum_{i=1}^{L} z_i(x_{ki})$$

as the realization of the three-dimensional random field.

The question that arises is "what is the form of the unidimensional covariance function $C_1(\xi)$ so that the field has the imposed three-dimensional covariance function $C_s(r)$?

We take two points of the field having location vectors x_1, x_2, respectively. It is assumed that at each point the values of the field have zero mean.

$$C_s(x_1, x_2) = E[Z_s(x_1) Z_s(x_2)]$$

$$C_s(x_1, x_2) = \frac{1}{L} \sum_{i=1}^{L} \sum_{j=1}^{L} E[Z_i(x_{1i}) Z_j(x_{2j})]$$

Because the unidimensional realizations along two different lines are independent, the expected value $E[Z_i(x_{1i}) Z_j(x_{2j})]$ will be zero unless $i = j$. Thus this expression reduces to

$$C_s(x_1, x_2) = \frac{1}{L} \sum_{i=1}^{L} E[Z_i(x_{1i}) Z_i(x_{2i})]$$

$$C_s(x_1, x_2) = \frac{1}{L} \sum_{i=1}^{L} C_1(x_{1i}, x_{2i})$$

or

$$C_s(h) = \frac{1}{L} \sum_{i=1}^{L} C_1(h \cdot u_i)$$

where $h = x_2 - x_1$. If $r = |h|$:

$$C_s(r) = \lim_{L \longrightarrow \infty} \frac{1}{L} \sum_{i=1}^{L} C_1(h \cdot u_i)$$

By using the law of large number we obtain :

$$C_s(r) = E[C_1(h \cdot u)]$$

We define orthogonal (x, y, z) axes with origin at the point x_1 and with the z axis in the direction of the vector $h = x_2 - x_1$, as shown in figure 15.

$$C_s(r) = \frac{1}{4\pi} \int_0^{2\pi} \int_0^{\pi} C_1(r \cos\phi) \sin\phi \; d\phi \; d\theta$$

$$C_s(r) = \frac{1}{2} \int_0^{\pi} C_1(r \cos\phi) \sin\phi \; d\phi$$

Then by symmetry :

$$C_s(r) = \int_0^{\frac{\pi}{2}} C_1(r \cos\phi) \sin\phi \; d\phi$$

We introduce the line coordinate $\xi = r \cos\phi$ oriented in the direction of u. $d\xi = -r \sin\phi d\phi$

$$C_s(r) = \frac{1}{r} \int_0^{r} C_1(\xi) \; d\xi$$

Differentiating and changing notation leads to the relationship between one- and three-dimensional covariances :

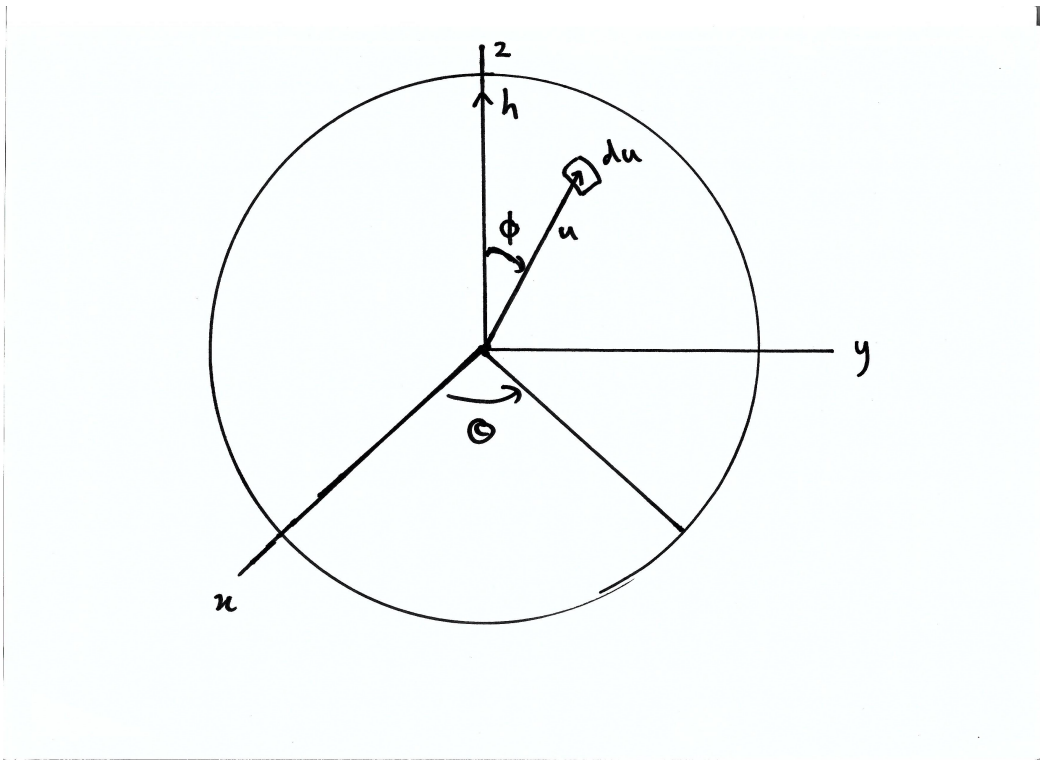

Figure 12: Turning bands method

$$C_1(\xi) = \frac{d}{d\xi}\xi C_s(\xi)$$

.

Example 3.1. *For an exponential three-dimensional covariance*

$$C_s(r) = \sigma^2 \exp(-br),$$

the corresponding one-dimensional covariance is

$$C_1(\xi) = \sigma^2(1 - b\xi)\exp(-b\xi),$$

commonly called the "hole function".

For a double exponential three-dimensional covariance

$$C_s(r) = \sigma^2 \exp(-b^2 r^2),$$

the corresponding one-dimensional covariance is

$$C_1(\xi) = \sigma^2(1 - 2b^2\xi^2)\exp(-b^2\xi^2).$$

For an spherical three-dimensional covariance

$$C_s(r) = \begin{cases} \sigma^2(1 - \frac{3br}{2} + \frac{(br)^3}{2}), & for\ 0 \leq br \leq 1 \\ 0 & for\ br > 1 \end{cases}$$

and the corresponding one-dimensional covariance is

$$C_1(\xi) = \begin{cases} \sigma^2(1 - 3b\xi + 2(b\xi)^3), & for\ 0 \leq b\xi \leq 1 \\ 0 & for\ b\xi > 1. \end{cases}$$

Two-dimensional fields

We define orthogonal axes (x, y) in the plane of the field, with origin at point x, and the y axis in the direction of the vector $h = x_2 - x_1$ as shown in Figure 13.

In polar coordinates we can write $h \cdot u = r\sin\theta$ and $du = d\theta$. The equation then becomes

$$C_s(r) = \frac{1}{2\pi}\int_0^{2\pi} C_1(r\sin\theta)d\theta$$

C_1 is an even function, thus by symetrie of sin :

$$C_s(r) = \frac{2}{\pi}\int_0^{\frac{\pi}{2}} C_1(r\sin\theta)d\theta$$

We set $\xi = r\sin\theta$. Then, $d\xi = r\cos\theta\ d\theta$ and :

$$C_s(r) = \frac{2}{\pi}\int_0^{r} \frac{C_1(r)}{(r^2 - \xi^2)^{\frac{1}{2}}}d\xi$$

This equation relates the two dimensional covariance function $C_s(r)$ to the corresponding unidimensional $C_1(\xi)$ along the turning band lines. It is an integral equation in which $C_1(\xi)$ cannot be directly expressed s a function of $C_s(r)$. Particular solutions though can be found for certain two-dimensional covariance functions.

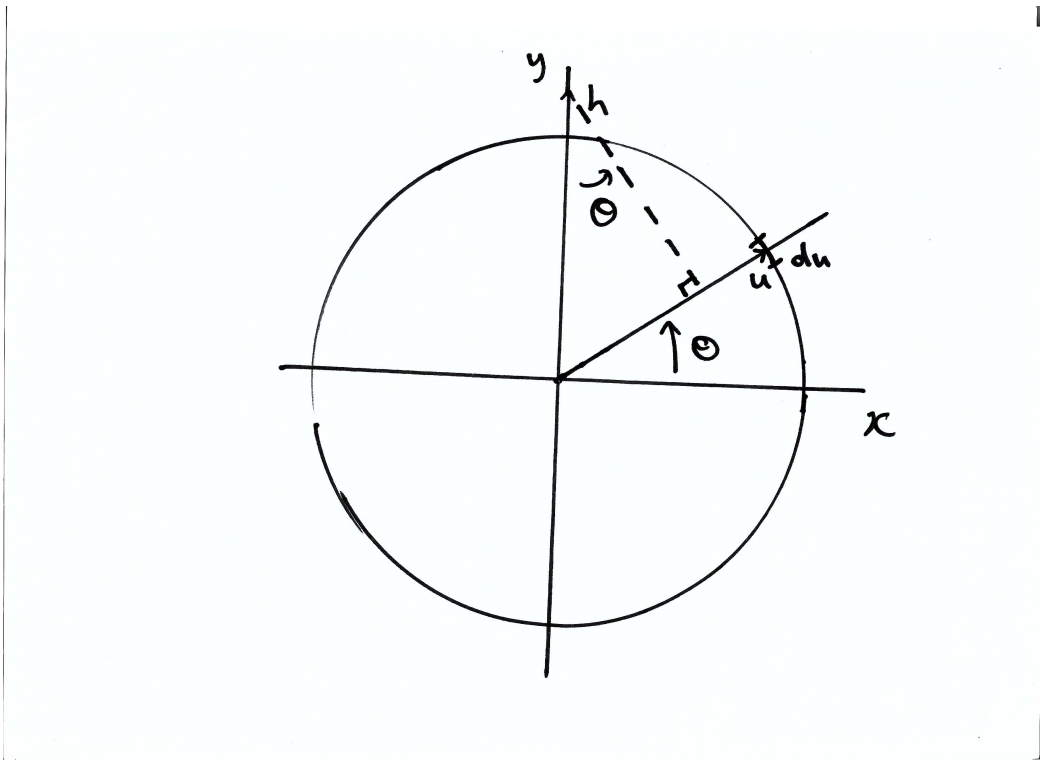

Figure 13: Turning band in 2D

3.3.1 Naive code of the turning bands method

```
library(Matrix)
library(rgl)
library(ggplot2)


cov_function <- function(s,b,r) {
  y <- s^2 * (1 - b * r) exp(-b*r)
  return(y)
}
###Corresponding one-dimensional covariance of a simple exponential

s <- 1
###Choose a value for s
```

```
b <- 1
###Choose a value for b

n <- 1000
### n is the number of points that we want to simulate
N<- 100
### N is the number of lines that we want to simulate

x <- runif(n,min =-1, max=1)
y <- runif(n,min =-1, max=1)
z <- vector("numeric", n)
### Gives us n points in the plan (x,y,0)

Z <- matrix(rep(z,N),nrow = n, ncol = N, byrow = TRUE)

Ux <- runif(N,min =-1, max=1)
### Gives us N vectors of lines
Uy <- runif(N,min =-1, max=1)
Uz <- runif(N,min =-1, max=1)

Points <- matrix(c(x, y, z), nrow=3, ncol=n, byrow=T)
Droites <- matrix(c(Ux, Uy, Uz), nrow=3, ncol=N, byrow=T)

A <- t(Points)%*%Droites
B <- diag(sqrt(t(Droites)%*%Droites))
C <- matrix(rep(B,n),nrow = n, ncol = N, byrow = TRUE)
D <- A/C
### Projection of the points on each line

i <- N
while (i > 0) {
  M <- matrix(rep(D[,i],n),nrow = n, ncol = n, byrow = TRUE)
### Matrix consisting of the vector a on each row
  N <- matrix(rep(D[,i],n),nrow = n, ncol = n, byrow = FALSE)
### Matrix consisting of the vector a on each column
  P <- M - N
  Q <- abs(P)
###Q_{ij} is the distance between a_i et a_j
```

```
  cov_mat <- cov_function(s,b,Q)
###Gives us a covariance matrix of covariance function cov_function
  lu <- lu(cov_mat)
  elu <- expand(lu)
  L <- elu$L
###L is the lower matrix of the LU decomposition
  X<-rnorm(n,mean=0,sd=1)
  Y=L%*%X
  Z[,i]<-Y[1:n]
###vector of the simulated values
  i <- (i - 1 )
}


Z
bis <- apply(Z,1,sum)
Val <- 1/sqrt(100)*bis
###Realization of the three-dimensional random field

res <- (Val - min(Val))
symbols(x,y,circles = res, inches = 0.2)

df <- data.frame(Valeur=Val)
ggplot(df, aes(x=Valeur)) + geom_histogram()
```

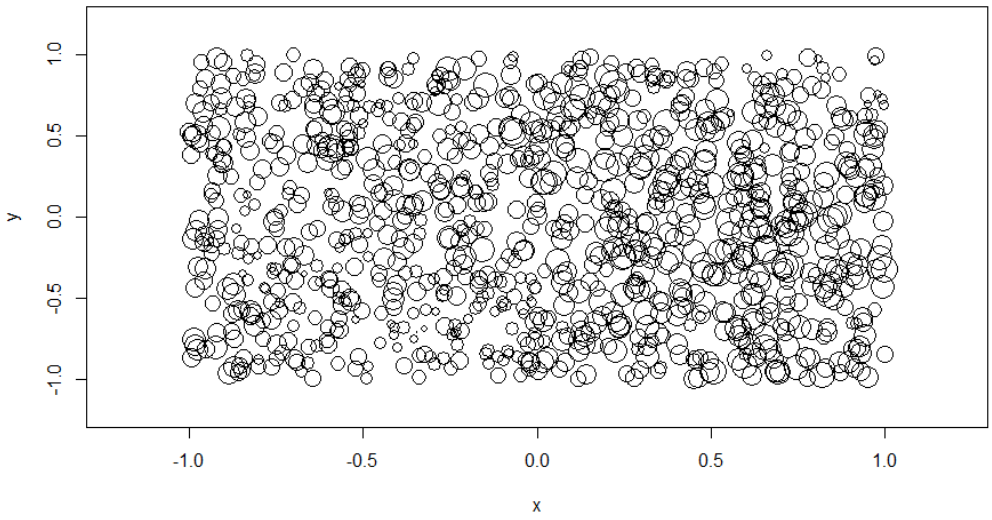

Figure 14: Illustration with exponential

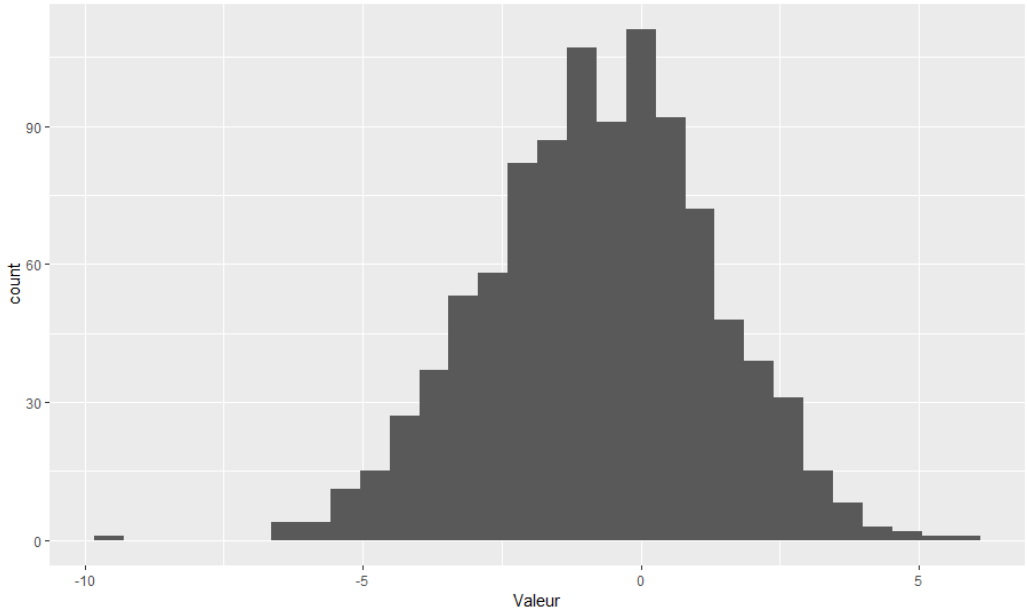

Figure 15: Histogram

3.3.2 Practical application of the Turning bands

The following simulations are realizations on a regular grid 51×51 on $[0, 200]^2$ of a centered gaussian process with different covariances but with the same parameters. Unlike the Cholesky decomposition, we cannot have the same shape of the random field because randomness intervene differently with the simulations of various directions.

Firstly we got, for each of the gaussian random fields which have different covariance functions, the same histogram of the value of $Z(\cdot)$ in accordance with the Figure 16. This histogram shows us that the distribution keeps effectively a gaussian distribution of average 0.

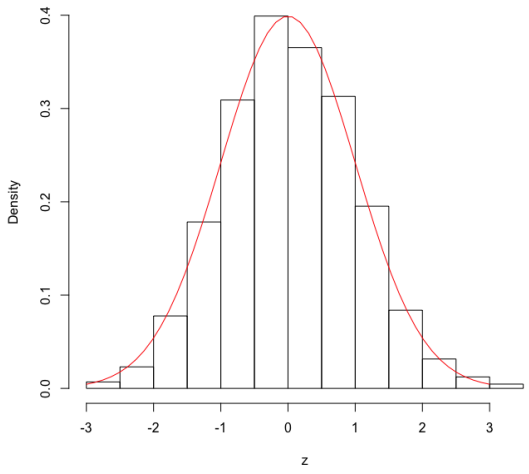

Figure 16: Histogram of $Z(\cdot)$

The pure nugget effect has the same shape of random field and the same variogram taking into account stochastic variations (Figure 17).

The Figure 18-a representing the gaussian random field of spherical covariance is approximately of the same shape as the Cholesky method: there is again a granular appearance of the field due to the covariance function. Finally, we observe that the experimental variogram is close to the theoretical variogram (Figure 18-b). The remarks are similar for the exponential covariance and its gaussian random field (Figure 19-a,b).

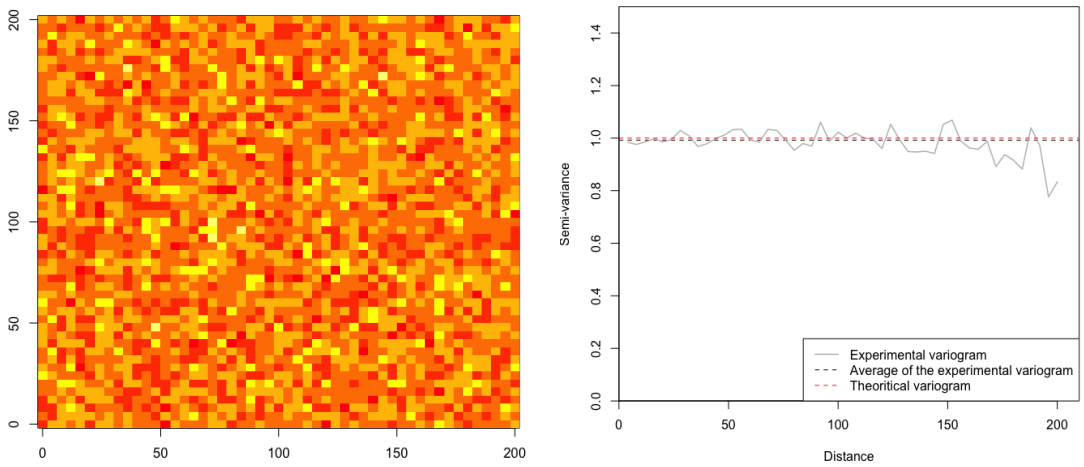

(a) (b)

Figure 17: Pure nugget effect (a) gaussian random field and (b) variogram with sill = 1.

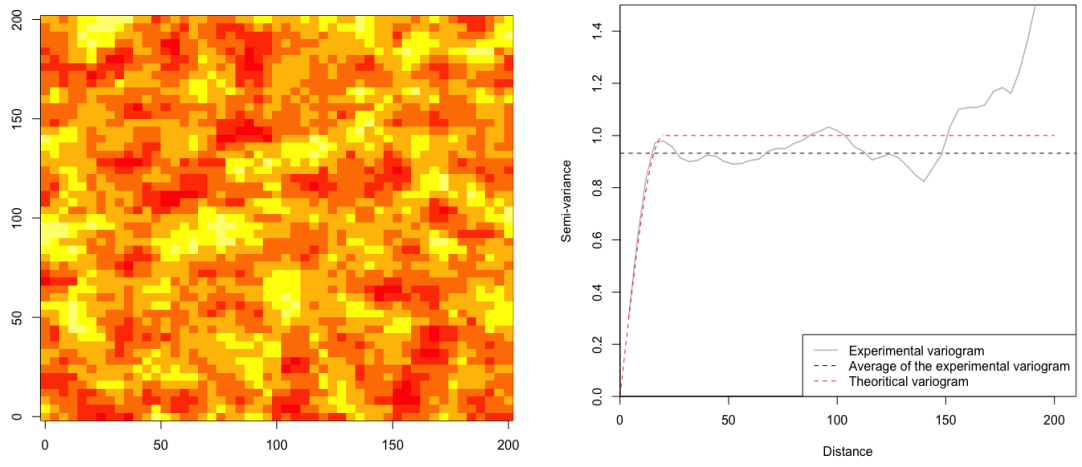

(a) (b)

Figure 18: (a) Gaussian random field and (b) variogram of spherical covariance with nugget = 0, sill = 1 and range = 20.

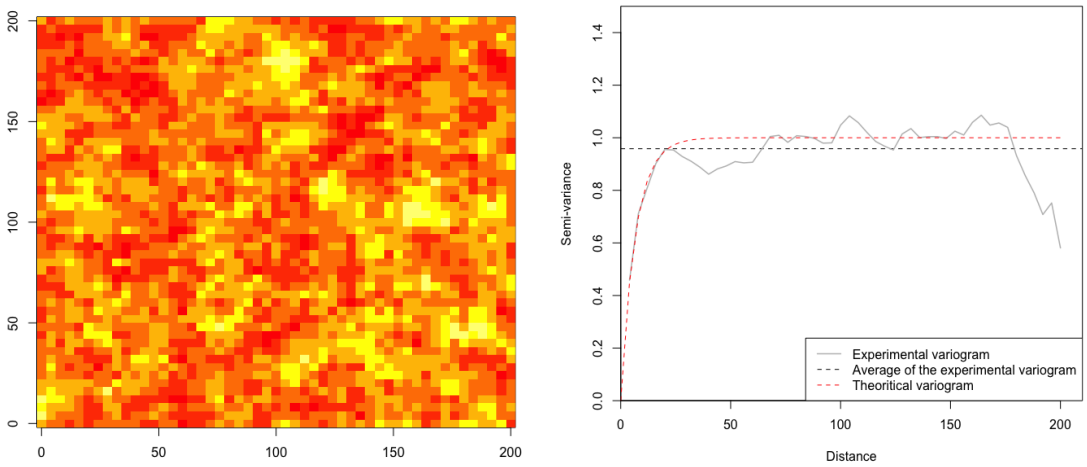

(a) (b)

Figure 19: (a) Gaussian random field and (b) variogram of exponential covariance with nugget = 0, sill = 1 and range = 20.

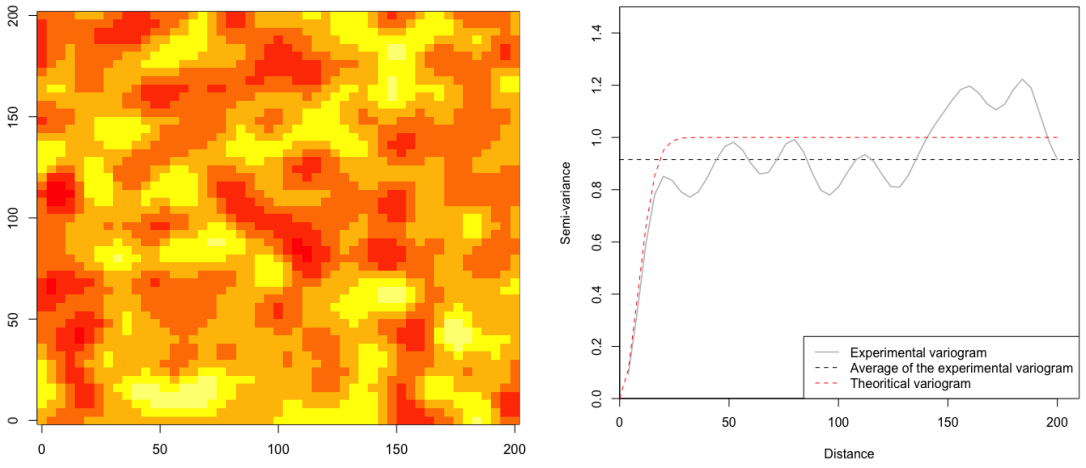

(a) (b)

Figure 20: (a) Gaussian random field and (b) variogram of gaussian covariance with nugget = 0, sill = 1 and range = 20.

The Figure 20-a is similar to the field obtained by the Cholesky method. The high regularity at the origin causes the blurred aspect or a gathering aspect. We observe on the Figure 20-b that the experimental variogram varies much more near the sill than the one obtained by the Cholesky method, and it is explained by the stochastic part of the simulation. Indeed, after simulating further fields and their variograms, the result was that the variograms tends to the theoretical variogram. This is what we will show in the next subsection.

In order to compare the calculation time of each method, we used the function `proc.time()`. For the Cholesky decomposition, the elapsed time was 3.070 seconds. For the Turning bands method, the elapsed is 0.021 second, which is largely better than the previous one.

The comparison between the Cholesky decomposition method and the Turning bands method is evident. The first method is demanding in terms of computing performance and the result is that some covariance function are quickly unusable due to the approximations.

3.3.3 Empirical convergence of the experimental variograms

The Figure 21 is a simulation of variograms for 3 different ranges (28, 80 and 160) of 20 gaussian random fields each time with an exponential covariance. Through this simulations, we traced the theoretical variograms, the average of the 20 experimental variograms and the confidence interval of them. The observations are similar to those gave for the Cholesky method. We observe already with only 20 fields that the experimental variograms converge empirically (in average) to the theoretical variogram. Moreover, we see that the confident interval is closer to the average variogram when the range is small compared to the dimension of the field.

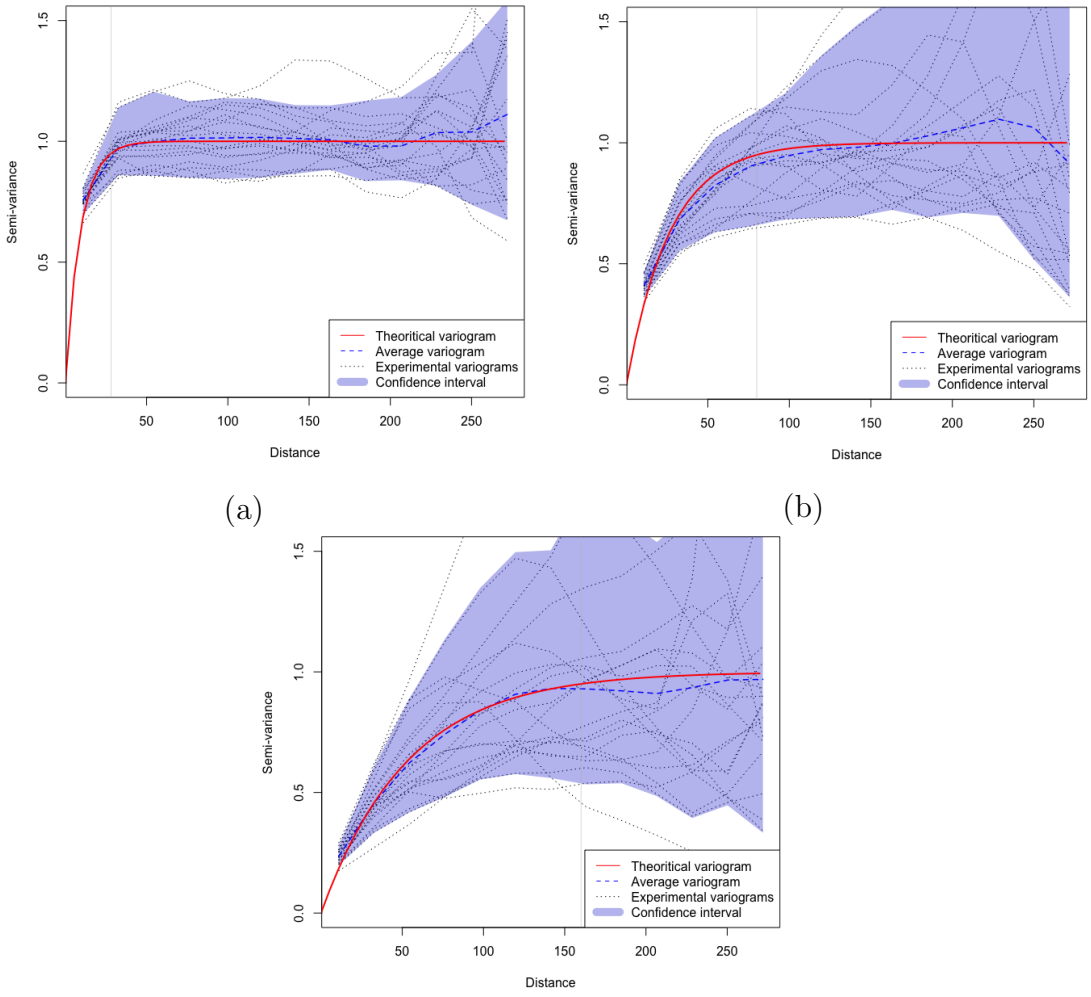

Figure 21: Averages of 20 exponential variograms with three practical ranges: (a) 28, (b) 80 and (c) 160.

4 Conclusion

Though the simulations done in this report, we can affirm that the Turning bands method is the better compared to the Cholesky decomposition method to simulate a gaussian random field from a performance point of view.

Furthermore, the result obtained for each method is the same finally, because the experimental variograms converge empirically to the theoretical variogram. Thus, the theoretical structure of the gaussian random field is well respected empirically. An opening to our work could be to introduce the integral range [5] which would facilitate the comparison of the different covariances. We could also introduce anisotropy which would change the way to analyze the variograms [1][3].

List of Figures

List of Tables

References

[1] Jean-Paul Chilès and Pierre Delfiner. *Geostatistics: Modeling Spatial Uncertainty*. Wiley edition, 1999.

[2] Jean-Jacques Droesbeke, Michel Lejeune, and Gilbert Saporta. *Analyse statistique des données spatiales*. Technip edition, 2006.

[3] Marian Eriksson and Peter P.Siska.

[4] Carlo Gaetan and Xavier Guyon. *Modélisation et statistique spatiales*. Springer edition, 2008.

[5] Christian Lantuéjoul. *The integral range*. Springer edition, 1973.

[6] Georges Matheron. *Les variables régionalisées et leur estimation*. Masson et cie edition, 1965.

[7] Georges Matheron. *The theory of regionalized variables and its applications*. Les cahiers du centre de morphologie mathématique de fontainebleau edition, 1970.

[8] Georges Matheron. *The intrinsic random functions and their applications*. Advances in applied probability, vol. 5, p. 439-468 edition, 1973.

[9] Carl Edward Rasmussen. *Gaussian Processes for Machine Learning*. The mit press edition, 2006.